Engineering Innovations
ISSN: 2813-1002, Vol. 9, pp 15-21
doi:10.4028/p-ShG23P

Submitted: 2023-06-26
Accepted: 2023-07-17
Online: 2024-02-12

Use of Polyacrylonitrile as Anodic Artificial Solid Electrolyte Interphase for Aqueous-Based Zinc-Ion Batteries

Nutchaya Muangplod[1,a], Anongnat Somwangthanaroj[1,b*] and Soorathep Kheawhom[2,c]

[1]Polymer Engineering Laboratory, Department of Chemical Engineering, Faculty of Engineering, Chulalongkorn University, Bangkok 10330, Thailand

[2]Research Unit of Advanced Materials for Energy Storage, Faculty of Engineering, Chulalongkorn University, Bangkok 10330, Thailand

[a]6370089921@student.chula.ac.th, [b]anongnat.s@chula.ac.th, [c]soorathep.k@chula.ac.th

Keywords: Rechargeable aqueous zinc-ion batteries; Zinc anode; Polyacrylonitrile.

Abstract. Rechargeable aqueous zinc-ion batteries (ZIBs) have attracted attention for energy storage systems because of their high specific capacity, low cost, and safety. However, practical application of the zinc anode in mild acidic electrolytes is limited by several issues such as dendrite formation, corrosion, hydrogen evolution reaction, passivation and relatively low cycling performance. Coating the zinc anode with graphite (GP) can partially solve these issues and improves the cycling performance of ZIB. However, after long-term charge/discharge cycles, zinc tends to migrate and redeposit over the surface of GP owing to the electronic conductivity of GP particles. Thus, after long-term cycling, the issues mentioned are back. Fabrication of artificial solid electrolyte interphase (ASEI) on the surface of the zinc anode shows high potential for solving these issues. In this work, polyacrylonitrile (PAN) with zinc trifluoromethanesulfonate ($Zn(CF_3SO_3)_2$) (PANZ) as ASEI was coated on the GP layer onto the zinc anode (PANZ@GP@Zn), and compared with the anode having GP coated layers and pristine zinc anode. The coating layer was prepared by the doctor blading method. The result showed that the PANZ@GP@Zn anode can reduce zinc deposition over the anode surface when compared with the GP@Zn anode, leading to the high cycling stability of ZIBs and extending the battery's life.

Introduction

The demand for renewable energy has risen rapidly due to fossil fuels over-consumption and environmental pollution and global warming issues. However, renewable energy is difficult to store, transport and its fluctuating nature. Therefore, an energy storage system (ESS) has been developed to provide a more versatile and stable power supply for personal, household and industrial applications [1].

The most well-studied energy storage system and widely used in the energy market is lithium-ion batteries (LIBs), which can provide high energy density, and long cycle lifetime [2]. Nonetheless, commercial LIBs are still suffer from high cost due to the limited lithium resource and safety issues, also hinder their development for large-scale energy storage applications. Considering these limitations of LIBs, it is necessary to search for new battery technology based on high safety, low cost, and long cycle life [3].

Rechargeable aqueous zinc-ion batteries (ZIBs) have been considered as the promising alternative energy storage system due to their high theoretical capacity (820 mAh g^{-1}), high natural abundance, low cost, environmental friendliness, and high safety [4]. However, the practical application of the zinc anode in mild acidic electrolytes is limited by several issues such as dendrite formation, corrosion, hydrogen evolution, passivation on the zinc surface, which reduces coulombic efficiency and cycling performance of ZIBs [1, 4].

One of various carbon materials that is a good alternative for using in zinc anodes is graphite (GP) due to its homogeneous electric field distribution, abundant active sites, and satisfying

durability, leading to the enhancement on the cycling performance of ZIBs [5, 6, 10]. Hence, coating the zinc anode with graphite can partially solve these issues. However, after long-term charge/discharge cycles, zinc tends to migrate and redeposit over the surface of the carbon layer owing to a good electronic conductivity of carbon particles [3]. Thus, after long-term cycling, the mentioned issues are back.

Polyacrylonitrile (PAN) is a solid polymer electrolyte that is attractive for use in ZIBs due to its low cost, chemical stability, excellent thermal stability, high tensile strength and tensile modulus. The polar nitrile group (-CN) can provide coordination sites to bridge Zn^{2+} ions. Nevertheless, polyacrylonitrile has partially hydrophobicity (ionic conductivity ~10^{-4} S cm^{-1}), so it is improved by adding zinc trifluoromethanesulfonate ($Zn(CF_3SO_3)_2$) or ($Zn(TfO)_2$) to this polymer to increase its hydrophilicity and higher ionic conductivity [7]. Also, The $S–O^-$ anions of $Zn(CF_3SO_3)_2$ can react with Zn^{2+} ions [8]. Hence, Polyacrylonitrile with zinc trifluoromethanesulfonate are used as artificial solid electrolyte interphase (ASEI) on the surface of the zinc anode that can regulate zinc ion distribution and uniform nucleation sites for zinc deposition on the anode surface [9]. Thus, ASEI shows high potential for solving the tendency that zinc tends to migrate and redeposit over the surface of carbon.

In this study, polyacrylonitrile (PAN) with zinc trifluoromethanesulfonate ($Zn(CF_3SO_3)_2$) (PANZ) as ASEI was coated on the graphite (GP) layer onto the zinc anode (PANZ@GP@Zn), and the results were compared to the anode having graphite coated layers and bare zinc anode in rechargeable aqueous zinc-ion batteries.

Experimental Section

Materials. Graphite (GP) powder, <20 μm, polyacrylonitrile (PAN) (MW. 150,000 g/mol), zinc trifluoromethanesulfonate ($Zn(CF_3SO_3)_2$) was purchased from Sigma-Aldrich, n,n-dimethyl formamide 99.8% (AR/ACS grade) (DMF) was purchased from Loba Chemie, n-methylpyrrolidone (AR grade) (NMP) was purchased from Quality reagent chemical, poly(vinylidene fluoride) (Solef®PVDF) (MW. 180,000 g/mol) was purchased from Solvay, zinc sulfate 7-hydrate ($ZnSO_4•7H_2O$) (AR grade, MW 287.58 g/mol) was purchased from Kemaus, zinc foil (thickness: 0.05 mm), graphite foil (thickness: 0.05 mm), glass microfiber paper (GF/A, Whatman) and blank coin cell CR2025 as well as other materials were used as received.

Preparation of negative electrodes. The graphite was mixed with polyvinylidene fluoride (PVDF) in n-methylpyrrolidone (NMP) solution with the weight ratio of carbon: PVDF as a binder which was 80:20, that was prepared under stirring at room temperature until it was homogeneous. It was then pressed onto a Zn foil (thickness, 50 μm) by the doctor blading method, and dried at 80 °C for overnight in vacuum to evaporate the solvent. The PANZ layer preparation was to dissolve 1.0 g polyacrylonitrile (PAN) into 9.0 g dimethylformamide (DMF) under stirring (800 rpm) at 50 °C until the polymer completely dissolved, then 1.0 g zinc trifluoromethanesulfonate ($Zn(CF_3SO_3)_2$) was dissolved in the solution. It was then pressed onto GP@Zn which has been prepared before by the doctor blading method, and dried on the doctor blading machine at 55 °C for 3 h to evaporate the solvent. Finally, anode sheet was obtained and cut into a circular shape with 15 mm in diameter. The thickness of the polymer coating layer was 7-9 μm.

Preparation of positive electrodes. The δ-MnO_2 was chosen as a cathode for the battery. The δ-MnO_2 was made by dissolving 1.98 g of $KMnO_4$ in 60 mL of deionized (DI) water. Then, $MnSO_4.H_2O$ (0.336 g) was dissolved in 20 mL of DI water and dropped into the $KMnO_4$ solution, which had been stirred continuously for 30 minutes. The solution was transferred to a 100 mL Teflon autoclave and heated at 160 °C in an oil bath for 24 hours. The product was collected and cleaned with DI water. It was then dried at 80 °C for 12 hr. After the δ-MnO_2 was obtained, it was then mixed with other components as follows. The weight ratio of δ-MnO_2:super P:PVDF as a binder was 80:10:10 under stirring until it was homogeneous. It was then pressed onto a graphite (thickness, 50

μm) by the doctor blading method, and dried at 80 °C overnight in vacuum to evaporate the solvent. Finally, cathode sheet was obtained and cut into a circular shape with 15 mm in diameter. The batteries were fabricated as a CR2025 coin cell.

Material characterization. The morphology of the anode and separator surface images both initial and after cycling were obtained using the field emission scanning electron microscope (FE-SEM).

Electrochemical measurement. Electrochemical impedance spectroscopy (EIS) and Tafel curves were conducted via the potentiometer on three electrodes including bare and coated ones (bare Zn, GP@Zn and PANZ@GP@Zn) which were the working electrode, zinc foil was counter electrode and Ag/AgCl was reference electrode. The other electrochemical performances were investigated with CR2025 coin cells consisting of a working electrode, a counter electrode, and glass microfiber wetted with 2 M $ZnSO_4$ electrolyte for symmetrical Zn cells and 2 M $ZnSO_4$+0.5 M MnO_4 electrolyte for full cells. Electrochemical impedance spectroscopy (EIS) measurements were carried out with VersaSTAT tool over the frequency range between 100,000 Hz and 0.1 Hz with an AC voltage of 10 mV and indicated the electronic and ionic conductivities. The Tafel curves of bare Zn, GP@Zn and PANZ@GP@Zn measured in 2 M $ZnSO_4$ at a scan rate of 0.2 mV s^{-1}. This test was evaluated the corrosion and hydrogen evolution reaction on the anode surface. The galvanostatic charge/discharge cycling was performed on battery-testing system. The symmetrical cell with the bare Zn, GP@Zn and PANZ@GP@Zn was to evaluate the striping/plating performance of batteries. The long-term cycling performance and cycling stability of the zinc anodes were measured at a current density of 1 mA cm^{-2} with fixed capacity of 1 mAh cm^{-2}. The coulombic efficiency (CE) was the percentage of discharging capacity compared with the charging capacity to evaluate the battery's reversibility. The CE of half cells were measured at a current density of 1 mA cm^{-2} with fixed capacity of 1 mAh cm^{-2}. The rate capability of the full batteries were carried out at current densities of 50 mA g^{-1}, 100 mA g^{-1}, 200 mA g^{-1}, 500 mA g^{-1} and 200 mA g^{-1}, respectively. The current density and specific capacity values of the electrodes were normalized to the mass of δ-MnO_2.

Results and Discussion

The cross-sectional field emission scanning electron microscopy (FE-SEM) images of PANZ@GP@Zn as shown in Figure 1A was used to inspect the morphologies of the anode surface and thickness of coating layer before charging/discharging process, in which it was found that thickness of the PANZ layer and the graphite layer were 7-9 μm and approximately 93 μm, respectively. To test the impedance and ionic conductivity of zinc electrodes with bare Zn, graphite coated zinc (GP@Zn) and zinc was coated with the PANZ and graphite (PANZ@GP@Zn) in concentrated aqueous electrolyte of 2 M $ZnSO_4$. As shown in Figure 1B The Nyquist curves of impedance spectra of the different anodes before cycling presented the PANZ interfacial coating layer (PANZ@GP@Zn) reduced the impedance of the zinc anode more than the graphite layer (GP@Zn) and without coating layer (bare Zn). The result showed the PANZ@GP@Zn had the highest ionic conductivity, which implied that the fast Zn^{2+} transport through the PANZ layer. The anticorrosion capability of coating layer on anode and the effect of the PANZ coated graphite and graphite coated on the zinc corrosion were analyzed by Tafel curves in an electrolyte of 2 M $ZnSO_4$ as shown in Figure 1C. Compared to the bare Zn, the corrosion potential of PANZ@GP@Zn and GP@Zn increase from -0.9613 V to -0.9465 V and from -0.9613 V to -0.9510 V, respectively. The result showed more positive corrosion potential that indicates less tendency of corrosion reactions and hydrogen evolution reaction [7, 11]. Moreover, the PANZ layer also reduced the corrosion current. Thus, the PANZ@GP@Zn has a lower corrosion rate. When compared GP@Zn, the PANZ layer had the more positive corrosion potential, which indicated that the PANZ layer tends to be more corrosion resistant than GP@Zn.

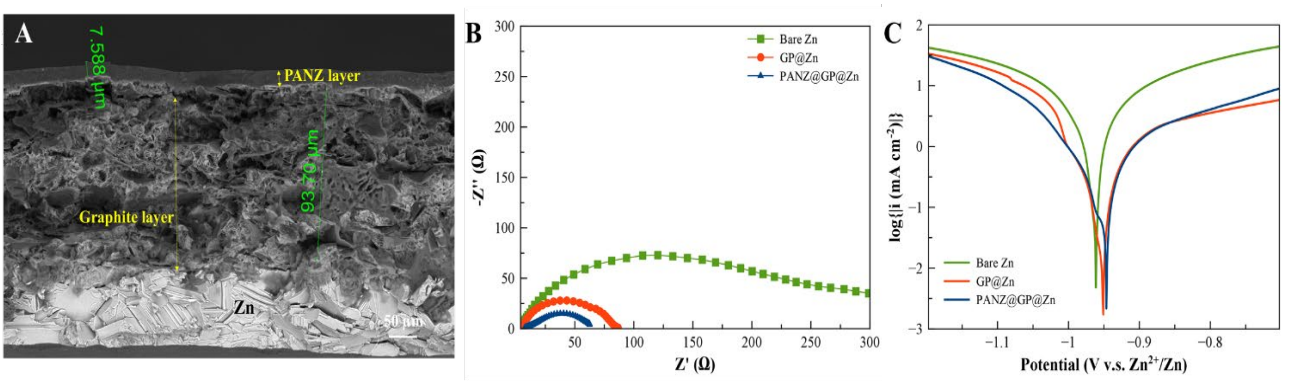

Fig. 1. Morphology analysis of PANZ@GP@Zn electrodes, EISs and Tafel curves of different zinc anodes. A) Cross-section view FE-SEM image of PAN@GP@Zn electrode before charging/discharging process. B) Electrochemical impedance spectra (EIS) of symmetric cells with bare Zn, GP@Zn and PANZ@GP@Zn anodes before cycling test. C) Tafel curves of bare Zn, GP@Zn and PANZ@GP@Zn in 2 M $ZnSO_4$ electrolyte.

The morphologies of the bare Zn, GP@Zn and PANZ@GP@Zn electrodes before cycling and after 100 cycles was examined by FE-SEM as shown in Figure 2. The FE-SEM images displayed the morphologies of the electrodes before cycling. The morphology of bare Zn in Figure 2A had quite smooth surface but some area had rough surface. The morphology of graphite coated Zn (GP@Zn) in Figure 2B showed the rough surface with considerable voids. The morphology of the PANZ layer and graphite coated Zn in Figure 2C showed micropores over the surface. However, after 100 charge/discharge cycles, the bare Zn cell was covered all over by corrosion pits, Zn dendrites as shown in Figure 2D. The formation of dendrites is also problem of Zn anode because inactive dendrite can block the transfer of ions and slow the ion diffusion process, while the GP@Zn in Figure 2E cell showed zinc deposit over the surface of graphite layer caused by zinc migrated from interface between the zinc anode and the graphite layer onto the graphite layer due to good electronic conductivity of graphite particles. In contrast, the PANZ@GP@Zn cell as shown in Figure 2F found slightly zinc on the surface of polymer layer caused by zinc deposited between the graphite surface and the PANZ layer. Compared to the carbon layer, the PANZ layer can reduce zinc deposition over the anode surface.

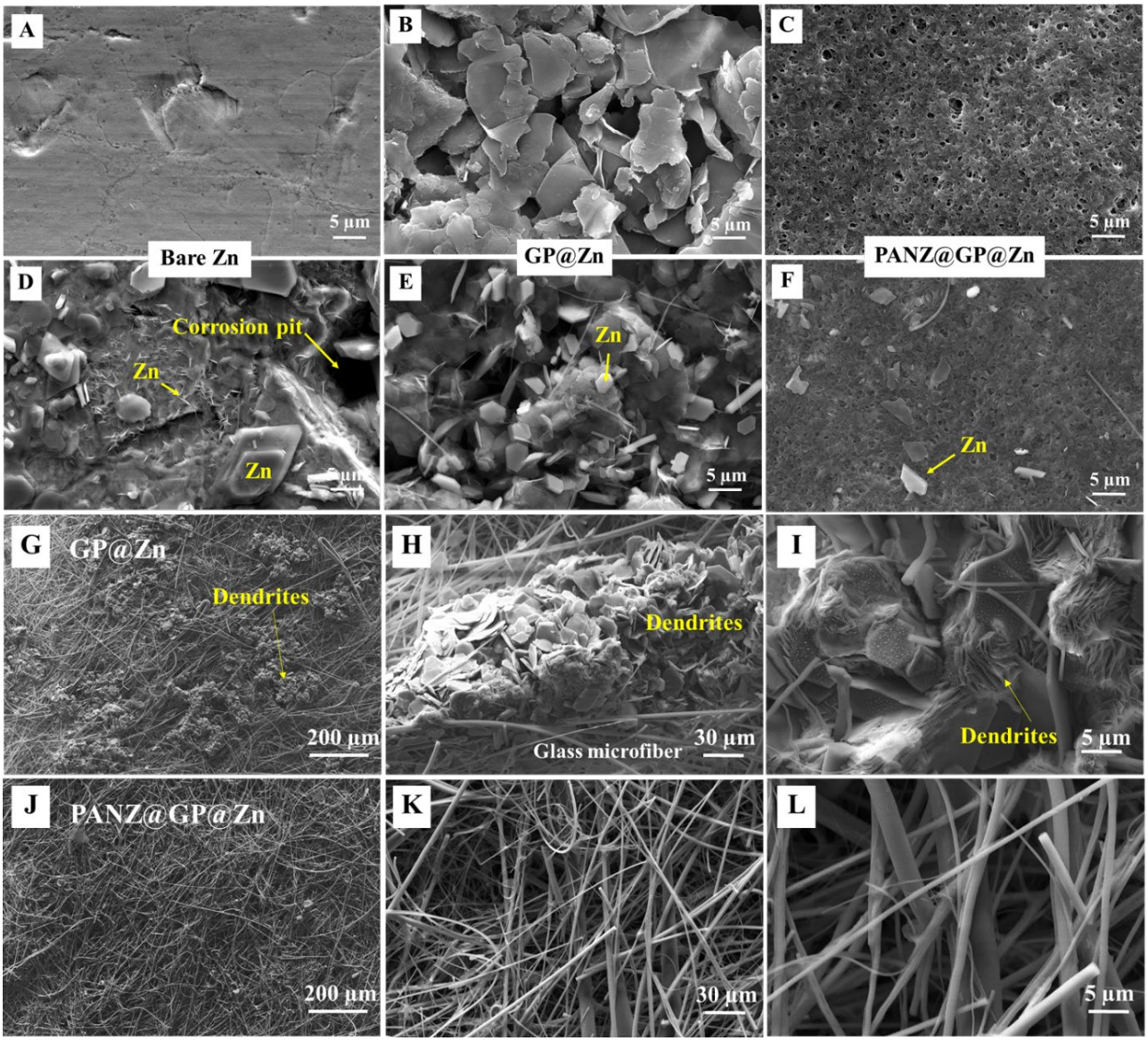

Fig. 2. Morphologies of electrodes and separators disassembled from symmetrical cell. Top view FE-SEM of images of Zn electrode with bare Zn, GP@Zn and PANZ@GP@Zn (A, B, C) before the cycling test, (D, E, F) after 100 cycles. Top view FE-SEM of images of glass microfiber separators with G-I) GP@Zn and J-L) PANZ@GP@Zn after 100 cycles at a current density of 1 mA cm^{-2} with 1 mAh cm^{-2}.

The morphologies of glass microfiber separator disassembled from the symmetrical cell with GP@Zn electrode, PANZ@GP@Zn electrode after 100 cycles at a current density of 1 mA cm^{-2} with 1 mAh cm^{-2}. As shown in Figure 2J, 2K and 2L, the glass microfiber separator of PANZ@GP@Zn electrode showed glass microfiber without dendrite. The separator of GP@Zn electrode as shown in Figure 2G and 2I showed flake-shaped dendrites spread on the separator surface and the separator pierced by dendrites as shown in Figure 2H, leading to the internal short circuit in the cell.

To evaluate the stability of symmetrical Zn cells with bare Zn, GP@Zn and PANZ@GP@Zn were assembled with 2 M $ZnSO_4$ and inspected with the galvanostatic charge/discharge cycling test. After 25 cycles (50 hours) at a current density of 1 mA cm^{-2} with a capacity of 1 mAh cm^{-2} as shown in Figure 3A, the cycling curve of bare Zn cell showed serious fluctuation and short circuit at 35 cycles (70 hours), which was inhomogeneous current distribution caused by the surface morphologies of bare Zn change during the charging/discharging processes of ZIBs due to dendrites, corrosion pits, hydrogen gas bubble found on the surface of bare Zn (Figure 2D) [5, 10]. On the other hand, the cycling curve of graphite coated Zn cell (GP@Zn) demonstrated more stable cycling than bare Zn

but the GP@Zn had reduced polarization voltage from 0.0390 V to 0.0186 V, which implied that the GP@Zn had migrated of Zn ions from the interface surface between Zn foil and the graphite layer to redeposition over the surface of graphite owing to good electronic conductivity of graphite particles [3]. Thus, the cycling curve of GP@Zn exhibited short circuit at 85 cycles (170 hours) because glass microfiber separator pierced by dendrites. In contrast, the PANZ@GP@Zn showed very stable curves during 250 cycles (500 hours) caused by the PANZ layer (Polyacrylonitrile with zinc trifluoromethanesulfonate) as ASEI which can regulate zinc ion distribution and uniform nucleation sites for zinc deposition on the anode surface, leading to suppressing side reactions and high cycling stability of ZIBs [7]. Therefore, the PANZ@GP@Zn cell has the most stability cycling and long-term cycling than bare Zn and GP@Zn cell.

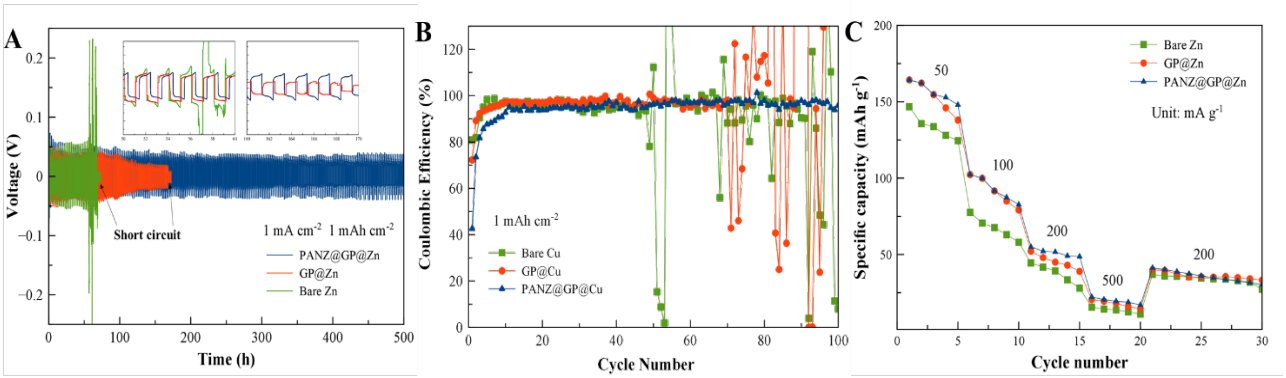

Fig. 3. Long-term cycling stability of symmetrical cells, the coulombic efficiency (CE) and Rate capability. A) The cycling performance of the symmetrical cells with bare Zn, GP@Zn and PANZ@GP@Zn at a current density of 1 mA cm^{-2} with 1 mAh cm^{-2}. B) The coulombic efficiency (CE) of Zn plating/stripping in the Cu-Zn, GP@Cu-GP@Zn and PANZ@GP@Cu-PANZ@GP@Zn half cells. C) Rate capability of full batteries from 50, 100, 200, 500 and 200 mA g^{-1} based on the mass of δ-MnO_2.

To investigate the effect of the PANZ coating layer and graphite layer on the coulombic efficiency (CE) of the reversibility of the Zn/Zn^{2+} process. During each cycling, Zn was dissolved from the Zn metal as cathode and deposits onto the Cu as anode. The CE of half-cell with PANZ@GP@Cu||PANZ@GP@Zn was evaluated and compared with bare Cu||bare Zn and GP@Cu||GP@Zn cells. The test was carried out by plating zinc (fixed areal capacity: 1 mAh cm^{-2}) onto the Cu, GP@Cu and PANZ@GP@Cu substrate. As displayed in Figure 3B, fluctuant voltage signals during Zn plating/stripping were observed with the bare Cu and the GP@Cu electrode because of side reactions. On the other hand, the PANZ@GP@Cu cell presented a very stable coulombic efficiency (CE) over 100 cycles (200 h), maintaining an average CE of 98.11% from cycle 10 (90.57%) to 100 (97.72%).

Full prototype cells were assembled to prove the practical application of our electrode. One of the most commonly used cathodes for aqueous ZIBs was delta-MnO_2 (δ-MnO_2), the δ-MnO_2 was investigated to further evaluate the impact of the PANZ coating layer and graphite layer on the electrochemical performance of full batteries consisting of bare Zn||δ-MnO_2, GP@Zn||δ-MnO_2 and PANZ@GP@Zn||δ-MnO_2 cells. The cells were charged/discharged in 2 M $ZnSO_4$ + 0.5 M $MnSO_4$ electrolyte, and $MnSO_4$ additive was used to suppress the dissolution of Mn^{2+} from the cathode [11, 12]. The rate capability of the bare Zn||δ-MnO_2, GP@Zn||δ-MnO_2 and PANZ@GP@Zn||δ-MnO_2 batteries were also tested at various current densities ranging from 50, 100, 200, 500 and 200 mA g^{-1}. As shown in Figure 3C, the rate capability of the PANZ@GP@Zn||δ-MnO_2 was better than that of GP@Zn||δ-MnO_2 and Zn||δ-MnO_2, which implies that PANZ@GP@Zn can reduce the fading of capacity than other anodes.

Summary

In this work, using polyacrylonitrile with zinc trifluoromethanesulfonate as ASEI on the graphite (GP) layer onto the zinc anode (PANZ@GP@Zn). Compare with the anode having graphite coated layers (GP@Zn) and bare zinc anode in rechargeable aqueous zinc-ion batteries (ZIBs). The PANZ@GP@Zn can increase ionic conductivity and less tendency of corrosion reactions and hydrogen evolution reaction. Moreover, the PANZ layer can reduce zinc deposition over the anode surface when compared with the carbon layer, leading to suppressing side reactions. Thus, the PANZ@GP@Zn has high cycling stability, long-term cycling performance of ZIBs and extending the battery's life**.** To identify the practical application, the PANZ@GP@Zn is suitable anode that can reduce the fading of capacity.

References

[1] Z. Yi, G. Chen, F. Hou, L. Wang, J. Liang, Strategies for the stabilization of Zn metal anodes for Zn-ion batteries, Advanced Energy Materials. 11(1) (2021) 2003065.

[2] W. Du, E.H. Ang, Y. Yang, Y. Zhang, M. Ye, C.C. Li, Challenges in the material and structural design of zinc anode towards high-performance aqueous zinc-ion batteries, Energy & Environmental Science. 13(10) (2020) 3330-3360.

[3] C. Li, X. Xie, S. Liang, J. Zhou, Issues and future perspective on zinc metal anode for rechargeable aqueous zinc-ion batteries, Energy & Environmental Materials. 3(2) (2020) 146-159.

[4] A. Bayaguud, Y. Fu, and C. Zhu, Interfacial parasitic reactions of zinc anodes in zinc ion batteries: underestimated corrosion and hydrogen evolution reactions and their suppression strategies, Journal of Energy Chemistry. 64 (2022) 246-262.

[5] W. Li, K. Wang, M. Zhou, H. Zhan, S. Cheng, K. Jiang, Advanced low-cost, high-voltage, long-life aqueous hybrid sodium/zinc batteries enabled by a dendrite-free zinc anode and concentrated electrolyte, ACS applied materials & interfaces. 10(26) (2018) 22059-22066.

[6] H. Tao, X. Tong, S. Zhang, X. Zhang, X. Liu, Effect of adding various carbon additives to porous zinc anode in rechargeable hybrid aqueous battery, Journal of Alloys and Compounds. 658 (2016) 119-124.

[7] P. Chen, X. Yuan, Y. Xia, Y. Zhang, L. Fu, L. Liu, N. Yu, Q. Huang, B. Wang, X. Hu, Y. Wu, T. van Ree, An Artificial Polyacrylonitrile Coating Layer Confining Zinc Dendrite Growth for Highly Reversible Aqueous Zinc-Based Batteries, Advanced Science. 8(11) (2021) 2100309.

[8] P. Chen, W. Zhou, X. Zhoujian, S. Li, Z. Wang, Y. Wang, An integrated configuration with robust interfacial contact for durable and flexible zinc ion batteries, Nano Energy. 74 (2020) 104905.

[9] F. Lorandi, T. Liu, M. Fantin, J. Manser, A. Al-Obeidi, M. Zimmerman, K. Matyjaszewski, J.F. Whitacre, Comparative performance of ex situ artificial solid electrolyte interphases for Li metal batteries with liquid electrolytes, Iscience. 24(6) (2021) 102578.

[10] Z. Li, L. Wu, S. Dong, T. Xu, S. Li, Y. An, J. Jiang, X. Zhang, Pencil drawing stable interface for reversible and durable aqueous zinc-ion batteries, Advanced Functional Materials. 31(4) (2021) 2006495.

[11] Z. Zhao, J. Zhao, Z. Hu, J. Li, J. Li, Y. Zhang, C. Wang, G. Cui, Long-life and deeply rechargeable aqueous Zn anodes enabled by a multifunctional brightener-inspired interphase, Energy & Environmental Science. 12(6) (2019) 1938-1949.

[12] C. Qiu, X. Zhu, L. Xue, M. Ni, Y. Zhao, B. Liu, H. Xia, The function of Mn^{2+} additive in aqueous electrolyte for Zn/δ-MnO_2 battery, Electrochimica Acta. 351 (2020) 136445.